Vortex interaction with a moving sphere

J. J. ALLEN[1], Y. JOUANNE[2] AND B. N. SHASHIKANTH[1]

[1]Department of Mechanical Engineering, New Mexico State University, NM, USA

[2]Department of Mechanical Engineering, l'Ecole Polytechnique, Université de Nantes, France

This paper details the experimental results of the axisymmetric collision of a vortex ring with a sphere. The experiments were conducted in water and a neutrally buoyant sphere was free to move in response to the impulse delivered by the vortex ring during the interaction. Good agreement has been achieved between kinematic data for the sphere speed and acceleration and the behaviour of the moment and rate of change of the moment of vorticity, measured using particle image velocimetry (PIV). The interaction of the vortex ring with the sphere creates secondary vorticity on the sphere surface. This initially results in a reduction of the fluid impulse and an acceleration of the sphere. However, within the measurement window of the interaction, the rate of increase of the positive moment of vorticity is slightly larger than the rate of increase of the negative moment of vorticity and the sphere gradually slows. A movie is available with the online version of the paper.

1. Introduction

Vortex rings have fascinated researchers for centuries because of their ease of formation and the complexity of results they produce. The study of vortex rings and ring interactions can give physical insights to more complicated flow fields that are dominated by coherent vorticity such as fluid/structure interactions. Forces on structures can be obtained by considering the evolution of the vorticity field, see Lighthill (1986). Secondary vorticity, which is produced when a vortex moves over a surface, can substantially alter the dynamics of the interaction when compared to an inviscid analysis. To illustrate this point consider the interaction of a vortex ring with a plane stationary surface. Inviscid analysis predicts that as the ring approaches the surface its diameter increases asymptotically to infinity as the distance between the ring core and the surface approaches zero. In reality, viscous effects are important, and as the ring approaches the surface considerable secondary vorticity is generated on the surface to enforce the no-slip condition. If the Reynolds number of the ring is high enough this secondary vorticity separates from the surface and dynamically interacts with the primary ring resulting in the ring rebounding from the surface, see Walker *et al.* (1987), Orlandi & Verzicco (1993). Alternatively, if the Reynolds number is low and viscous effects are important, rebound will still occur but without the separation of the induced boundary layer, see Peace & Riley (1983).

Another simple experiment is the axisymmetric interaction of a vortex ring with a sphere that is free to respond to the vortex ring impulse. This experiment represents possibly the simplest possible interaction of a vortical patch of fluid with a moving body and was commented on by Kelvin (1868). It also represents a test case for inviscid models of force prediction and kinematic response of solid bodies that are
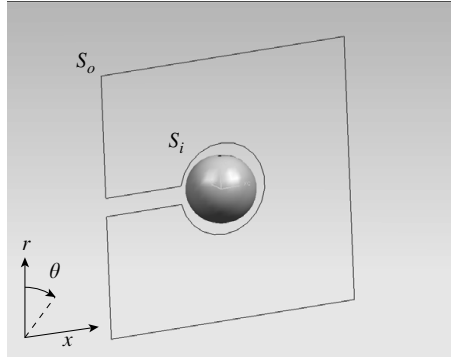
FIGURE 1. Sphere free-body diagram showing inner surface, S_i and outer surface S_o.

free to move in response to the pressure field created by coherent vorticity patches, see Shashikanth *et al.* (2002) and Shashikanth (2006) for further discussion of inviscid interaction models.

2. Background

The measurement of fluid loading on a body has historically been via the use of external gauges, such as strain gauges, with the body attached to a rigid sting. However, there are many practical situations where a body, such as a fish or bird, is accelerating/decelerating and it is desirable to compute the fluid loading without imposing external forces. In these situations it is advantageous to use non-intrusive methods to evaluate the forcing levels between the fluid and the body. This can be done by measuring the rate of change of the momentum of the fluid around the body and can be expressed in terms of vorticity moments, see Noca, Shiels & Jeon (1999).

The purpose of this paper is to evaluate the force on a sphere that is free to move in response to the fluid forcing. From the free body diagram in figure 1, the net force on the control volume is the surface integral of pressure and viscous stresses on the outer section, S_o, the inner section, S_i, and the umbilical. The force balance across the umbilical cancels. No external forces are acting on the control volume (this represents a simplification of the experimental configuration described in §3). Using the Reynolds transport theorem one is left with the following force–momentum balance:

$$F/\rho = -\frac{\mathrm{d}}{\mathrm{d}t} \int_{V(t)} \boldsymbol{u}\,\mathrm{d}V + \oint_{S_o(t)} \hat{\boldsymbol{n}} \cdot [-p\boldsymbol{I} + \boldsymbol{T}]\,\mathrm{d}s \qquad (2.1)$$

The sphere has a no-slip, no-fluid-penetration condition on its surface; p and $\boldsymbol{T}$ are the pressure field and viscous surface stress on the outer boundary of the control volume $S_o(t)$; $\boldsymbol{u}$ is the velocity field of the fluid inside the control volume measured in an inertial frame. The force F is the force that the fluid exerts on the sphere and represents the integration of the pressure field and surface shear stress over the inner control surface $S_i(t)$. Using the vector identity, obtainable from Stokes' theorem (see Saffman 1992 and Truesdell 1954),

$$\int_V \boldsymbol{x} \times (\nabla \times \boldsymbol{u})\,\mathrm{d}V = 2\int_V \boldsymbol{u}\,\mathrm{d}V + \oint_S \boldsymbol{x} \times (\hat{\boldsymbol{n}} \times \boldsymbol{u})\,\mathrm{d}S \qquad (2.2)$$

and neglecting the term $\oint_{S_o(t)} \hat{\boldsymbol{n}} \cdot [-p\boldsymbol{I} + \boldsymbol{T}]\,\mathrm{d}s$, whose contribution in our experimental set-up is small as the walls in the experiment are distant, equation (2.1) can be

transformed to

$$F/\rho = -\frac{1}{2}\frac{\mathrm{d}}{\mathrm{d}t}\int_{V(t)} \boldsymbol{x} \times \boldsymbol{\omega}\,\mathrm{d}V + \frac{1}{2}\frac{\mathrm{d}}{\mathrm{d}t}\int_{S_i(t)} \boldsymbol{x} \times (\hat{\boldsymbol{n}} \times \boldsymbol{u})\,\mathrm{d}S. \qquad (2.3)$$

The first term represents the time-varying moment of vorticity in the flow volume. In the case of bounded vorticity distributions, such as the vortex interacting with the sphere, the integration domain can be finite in size. The calculation of this integral requires knowledge of the time variation of the moment of vorticity distribution. The position vector $\boldsymbol{x}$ is grounded in an inertial frame. The second integral is related to the behaviour of the inner surface of the control volume. In the case of the moving sphere this integral is solved with knowledge of the temporal behaviour of the sphere. As the fluid no-slip condition applies at the surface of the inner control volume, $\boldsymbol{u}$ is equal to the sphere velocity. The first term in equation (2.3) is often referred to as the vortex force and the second term is related to the movement of the body, the added mass. If the interaction is axisymmetric and swirl-free, the motion of the sphere is along the x-axis, as defined in figure 1, then (2.3) reduces to the force on the sphere in the x-direction as

$$F_x/\rho = -\frac{1}{2}\frac{\mathrm{d}}{\mathrm{d}t}\int_{V(t)} (\boldsymbol{x} \times \boldsymbol{\omega})_x\,\mathrm{d}V - \frac{\mathrm{d}U_x(t)}{\mathrm{d}t}\frac{\pi D^3}{6} \qquad (2.4)$$

where D is the sphere diameter and U_x is the sphere velocity. The force the sphere experiences, F_x, can be considered to be decomposed into a force due to the vorticity distribution and an added mass force. This relationship has been noted previously in the study of loadings on a cylinder, see Govardhan & Williamson (2000) and Leonard & Roshko (2001).

3. Experiments

Experiments were conducted in the vortex ring generator tank described in Allen & Auvity (2002) with a water temperature of 20 °C. Brief details will be provided here. To produce a vortex ring a piston was moved through an 5.08 cm diameter acrylic tube. A plate was fixed to the end of the tube with a diameter of 4.15 cm. The speed of the piston was 4.6 cm s^{-1}. Particle image velocimetry (PIV) was used to measure the ring invariants: ring circulation Γ, impulse/density I and kinetic energy/density E. These groups are reorganized to form two non-dimensional parameters: the non-dimensional kinetic energy $\tilde{E} = E/(\Gamma^{3/2}I^{1/2})$ and the non-dimensional circulation $\tilde{\Gamma} = \Gamma/(I^{1/2}U_t^{2/3})$. U_t is the translational speed of the ring, see Allen & Naitoh (2005). Prior to running experiments that involved colliding the vortex ring with the sphere, measurements were made of the ring moving in the tank without the sphere being present. The non-dimensional energy of the ring was $\tilde{E} = 0.3$ and non-dimensional circulation was $\tilde{\Gamma} = 2.2$. The translational speed of the ring was 17 mm s^{-1} and the ring radius was 64 mm which results in a ring Reynolds number based on diameter and speed of $Re = 1147$. The Reynolds number based on the ring circulation was $\Gamma/\nu = 2275$ and the approximate (Norbury 1973) non-dimensional radius was $\alpha = 0.45$.

The sphere was suspended in the tank via a 4 m long, 0.2 mm thick fishing line. The section of the line supporting the sphere in the water tank was 0.07 mm thick Wollaston wire to minimize drag. By progressively releasing bubbles, conservatively estimated to have a diameter of order 2 mm the sphere was trimmed with light tapping to be slightly negatively buoyant. The sphere was able to be repeatedly

trimmed to within two bubbles of neutral buoyancy. The specific gravity of the sphere was estimated as 1.0004. The sphere was located 40 cm away from the vortex generator in an effort to have a ring at equilibrium, moving with steady velocity, before interacting with the sphere. The data collected during the interaction were:

(i) measurements of the trajectory of the sphere from video images;

(ii) flow visualization to measure the location of the vortex core during its interaction with the sphere;

(iii) PIV to measure the unsteady axisymmetric velocity field during the interaction. A detailed description of the PIV system used is contained in Allen & Smits (2001).

4. Results

4.1. *Flow visualization*

The sequence of flow visualization images in figure 2 shows the interaction of the vortex ring with the sphere. The visualizations were achieved using fluorescent dye in water and an argon-ion laser. The images in figures 2(*a*) and 2(*b*) show the ring deforming as it approaches the sphere. As the vortex passes around the sphere, significant secondary vorticity is generated on the surface of the sphere, which separates and evolves around the primary ring. This separated secondary vorticity can be seen clearly in figures 2(*c*) and 2(*d*). As the vortex ring passes over the sphere secondary vorticity is deposited in its wake as what appears to be a second vortex ring, figure 2(*e*) and (*f*). (A movie is available with the online version of the paper).

4.2. *Kinematic data*

Data for the location of the sphere and vortex core are shown in figure 3. The initial motion of the sphere, figure 3(*a*), is very repeatable; however as the sphere approaches its maximum displacement the curves become somewhat scattered. This was due to non-axisymmetric collisions. An axisymmetric collision, such as that shown in figure 2 was hard to achieve. When a perfect collision occurred it was very clear from experiments. In these cases the ring retained its coherent identity and progressed in the *x*-direction, albeit with a larger diameter, after it has passed around the sphere. The times listed for the flow visualization images, figure 2, and the trajectory data, figure 3, are synchronized. Figure 3(*b*) shows the mean curve for the displacement and the associated values for the sphere velocity and acceleration. It should be noted that the peak acceleration of the sphere occurs before the induced secondary vorticity separates from the sphere surface. Figure 3(*c*) shows data for the trajectory of the vortex core as it passes over the sphere. The ring diameter appears to reach an approximately constant value after it has passed the sphere that is order 50% larger than the original diameter. The production and separation of the secondary vorticity, figure 2(*b–d*), occurs when the sphere has reached a third of its maximum streamwise position.

4.3. *Effects of gravity and line drag*

The sphere diameter is 3.76 cm and its mass was 27.8 gms and hence the peak forces that are applied to the sphere during its motion are 7.8×10^{-5} N. An obvious question that arises concerns the role of the line tension and line drag on the sphere motion. For the images shown in figure 2(*a–d*) the sphere is displaced of order two diameters. With a line tension force of order 8×10^{-5} N, based on the sphere specific gravity, the force component that opposes displacement from equilibrium in the *x*-direction is order 2×10^{-6} N. The line supporting the sphere also has a drag component. If the
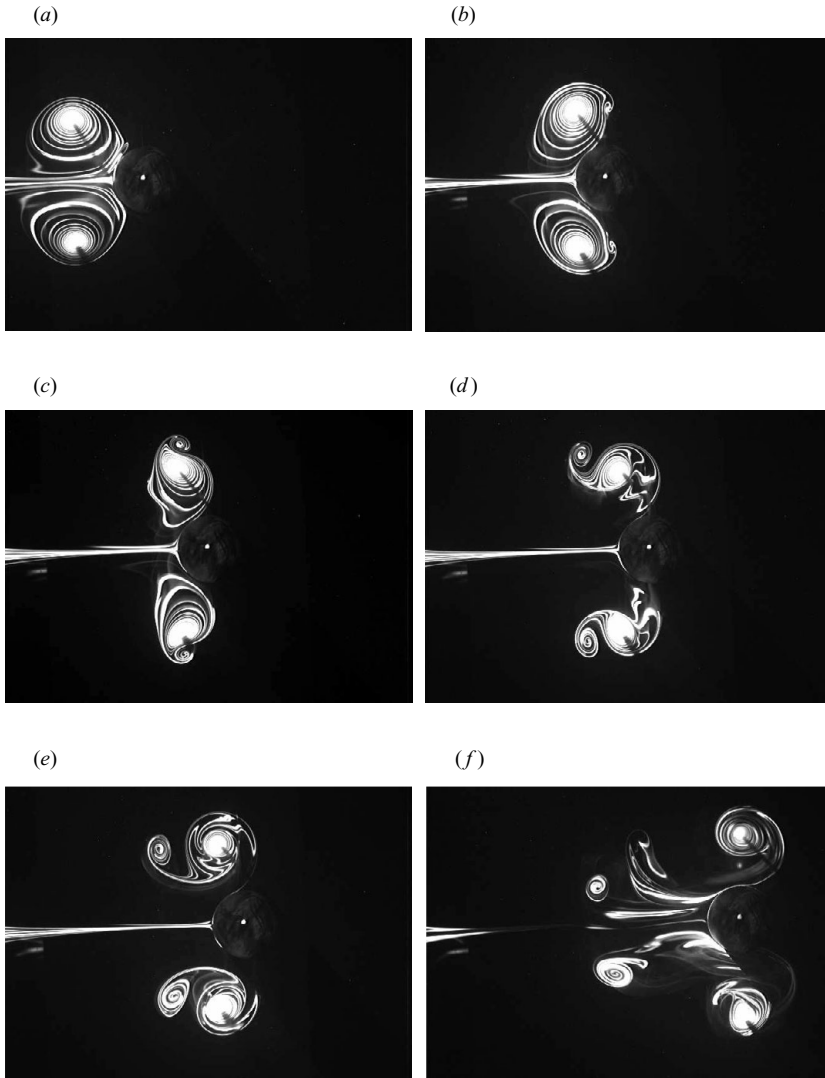
(*a*)

(*b*)

(*c*)

(*d*)

(*e*)

(*f*)

FIGURE 2. Dye visualizations at $t =$ (*a*) 9.3, (*b*) 11.0, (*c*) 11.9, (*d*) 12.7, (*e*) 13.6, (*f*) 17.8 s.

maximum speed of the Wollaston wire is taken as 1.5 cm s^{-1} it results in a Reynolds number of order unity and an associated drag coefficent of order ten. The associated drag force on the line is then order 7×10^{-6} N. Hence these two factors are small in terms of contributing to the sphere dynamics, even with conservative estimates.

4.4. *PIV*

A temporal sequence of PIV velocity fields were obtained with a time Δt between image pairs of 0.354 s. The measurement interval was selected such that it spanned the production and separation of the boundary layer from the sphere surface as the vortex ring passed around the sphere. Figure 4 shows the sequence of velocity fields and their associated vorticity fields. The azimuthal vorticity fields were generated by fitting a spline to the velocity data, as described in Allen & Chong (2000). The vorticity fields in figure 4 have been normalized as $\boldsymbol{\omega}_\theta = \boldsymbol{\Omega}_\theta D^2/\nu$. Figure 4(*a*) shows

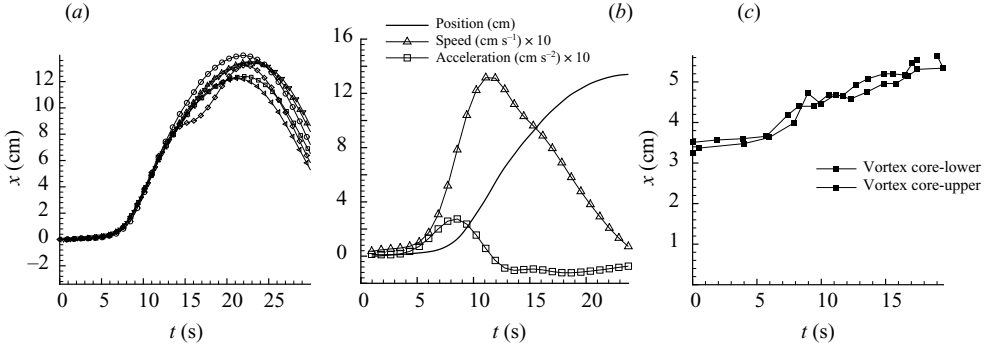*J. J. Allen, Y. Jouanne and B. N. Shashikanth*

FIGURE 3. (*a*) Trajectory, (*b*) velocity and acceleration of sphere, and (*c*) vortex core trajectory.

that as the vortex approaches the sphere it has produced an eruption of secondary vorticity from the sphere surface. As the interaction continues the vortex diameter increases in response to the presence of the sphere and the production of secondary vorticity on the sphere surface. The secondary vorticty can be thought to act as a 'virtual surface'. In figures 4(*b*) and 4(*c*) the secondary vorticity plume appears to wrap around the front of the advancing vortex. In figure 4(*d*) the secondary vorticity front appears to have pinched off, with the lead section of the front moving in the reverse direction to the vortex ring. The pinched-off section revolves as a satellite around the outside of the vortex ring core and is moving toward the ring wake. This phenomena can also be observed in the flow visualization images, figures 2(*d*) and 2(*e*). The remainder of the secondary front appears as a plume interacting with the vortex and retains its link with the sphere surface. In figures 4(*c*) and 4(*d*) the vorticity in the primary core has lost its elliptical form owing to the interaction with the secondary vorticity front. The overall levels of secondary vorticity strength are half to two-thirds that of the primary core, indicating it is dynamically significant.

4.5. *Correlation of experimental data with force balance equations*

As stated earlier, the goal of this work is to reconcile the kinematic motion of a body with the behaviour of the vorticity field it is interacting with. Using the stated assumption of the absence of a component of line tension, line drag and wall effects and using $F_x/\rho = (\mathrm{d}U_x/\mathrm{d}t) \cdot \pi D^3/6$ equation (2.4) becomes

$$\frac{D^3}{3}\frac{\mathrm{d}U_x}{\mathrm{d}t} = -\frac{\mathrm{d}}{\mathrm{d}t}\int\int \boldsymbol{\Omega}_\theta(r,\theta)r^2\,\mathrm{d}r\,\mathrm{d}x. \tag{4.1}$$

The integration of the moment of vorticity is performed over the fluid domain only. Reorganizing the integral in equation (4.1) into a non-dimensional form using the sphere diameter D and viscosity to normalize and then integrating with respect to time yields an expression for the non-dimensional velocity of the sphere:

$$u_x^*(t) = DU_x(t)/\nu = -3\int\int \omega_\theta^*(r^*,x^*)r^{*2}\mathrm{d}x^*\mathrm{d}r^* + \kappa \tag{4.2}$$

where the integral is performed over the fluid domain. Equation (4.2) is interpreted as the conservation of the combined linear momentum of the fluid plus the sphere. The constant of integration, κ, can be interpreted as the impulse (vorticity moment)
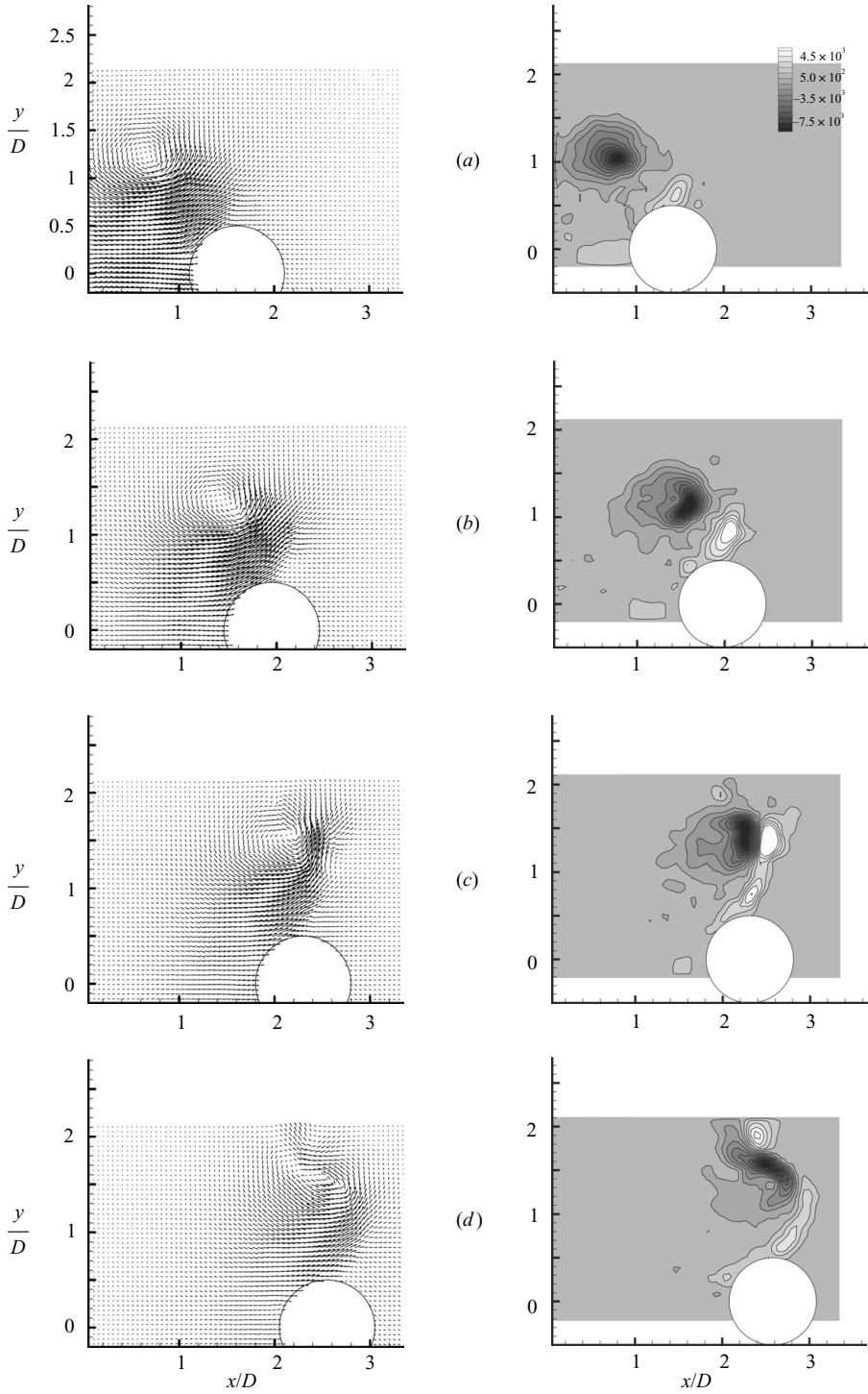
FIGURE 4. Velocity and associated vorticity fields for $t =$ (*a*) 10.1, (*b*) 10.7, (*c*) 11.6 and (*d*) 11.9 s.
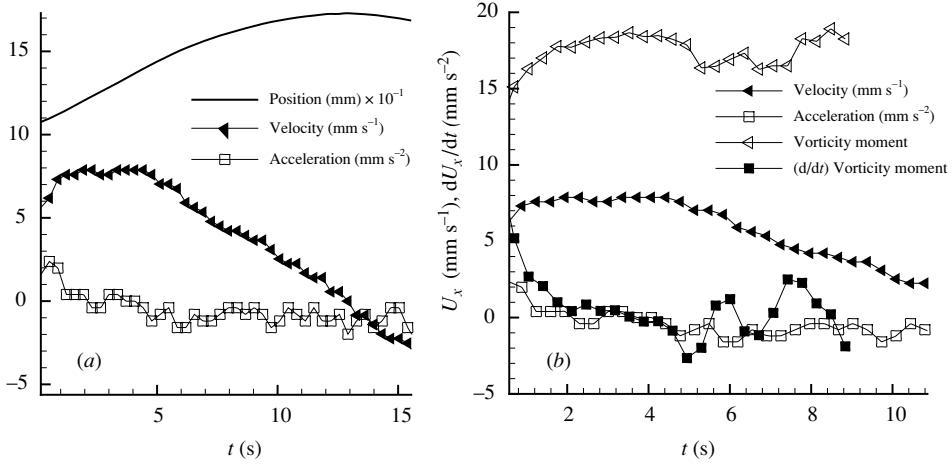
FIGURE 5. (*a*) Measured position, velocity and acceleration of sphere from PIV images and (*b*) comparison with vorticity moments and rates of change of vorticity moments.

of the vortex ring when the ring is remote from the sphere and the sphere essentially at rest, i.e. $u_x^* = 0$.

Figure 5(*a*) shows kinematic data for the sphere position, velocity and acceleration collected from the PIV images. Figure 5(*b*) shows the time-varying moment of vorticity integral compared with the ring speed over the time interval that all the coherent vorticity is in the PIV image plane. The general shape of the curves is the same; however the moment-of-vorticity curve is offset. This is a result of not knowing the value of the integration constant, κ. Figure 5(*b*) also shows a comparison of the acceleration of the sphere and the time rate of change of the vorticity moment. Agreement is good, within experimental error bounds. This also provides further evidence that the effects of gravity and line drag are minimal. The results for time rate of change of vorticity moment and sphere acceleration are obviously more noisy than the result for the vorticity moment and sphere velocity, but we have been relatively successful in evaluating indirectly the forcing levels on the sphere from measurement of the vorticity field.

To estimate the integral constant in equation (4.2) an experiment was conducted without the sphere in place, i.e. this represents the situation where the vortex ring is remote from the sphere and hence $u_x^* \simeq 0$. The normalized result for the vorticity moment integral was 411. Hence by adding this constant to the vorticity moment when the sphere and vortex interact we have a complete description of terms in equation (4.2) and good agreement with the data for the velocity of the sphere, figure 6(*a*). The non-dimensional time scale t^* in figure 6 has been normalized as $t\nu/D^2$. Error bounds have been shown on the data for vorticity moment. The main source of error in evaluating the moment comes from the measured vorticity. Other sources of error, such as establishing the time, centreline of interaction and moment arm radius are order 1%. The accuracy of the vorticity measure depends on the accuracy of the velocity measurement technique. With PIV we estimate the error in velocity as 3% using sub-pixel curve fits to the correlation function. Based on the spatial resolution of our velocity grid and the global spline technique of Spedding & Rignot (1993) we have an associated error in vorticity of order 15%.
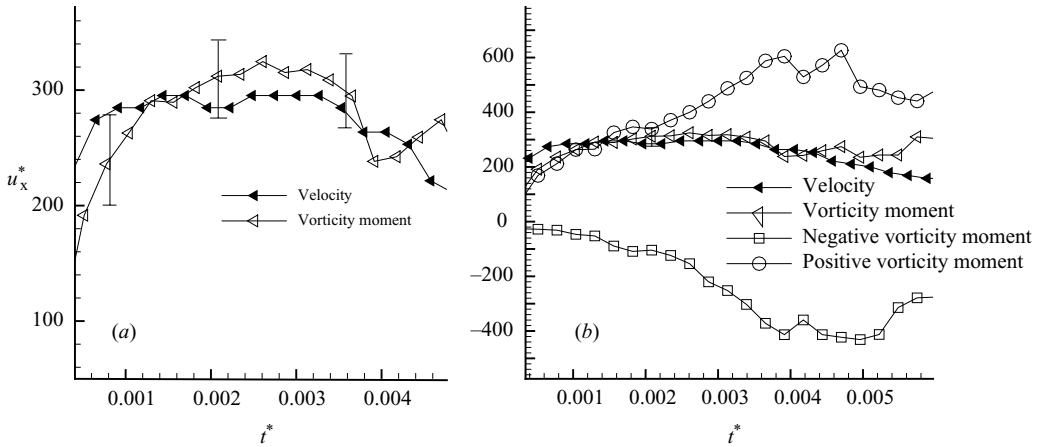
FIGURE 6. (*a*) Comparison of non-dimensional sphere velocity and that predicted from the vorticity moment and (*b*) behaviour of positive and negative components of the vorticity moment.

The role of the secondary vorticity in the dynamics of the interaction can be interpreted through the behaviour of the vorticity moment. Figure 6(*b*) shows the temporal behaviour of the moment of vorticity of the primary vortex ring and the moment of vorticity of the secondary vorticity plume. The viscous length scale, $\sqrt{\nu t}$, for the initial period of interaction of the vortex with the sphere and the eruption of secondary vorticity is order 1.5 mm. This is small in relation to the size of the vortices that are interacting and therefore we can consider the dynamics of the interacting patches from an inviscid standpoint. In order for the sphere to be accelerated to the right a negative rate of momentum loss of the fluid is required. Alternatively if we consider the interaction from the behaviour of impulse (velocity), as the sphere moves to the right from rest the fluid must have a reduction in impulse. This can be achieved in two ways via the moment of vorticity integral: either with the production of secondary vorticity on the sphere surface which will have the effect of increasing the vorticity moment integral and/or the modification of the path of the primary vortex. The primary vortex would need to reduce its diameter during its interaction with the sphere in order to reduce its negative contribution to the vorticity moment. This was not documented in figure 3(*c*). When the vortex ring is passing over the sphere its diameter is increasing, resulting in a reduction in the strength of the total vorticity moment. Both effects compete with each other while the ring is passing over the sphere. The velocity of the sphere shows a weak decrease, indicating that the dynamical effect of increasing the diameter of the primary ring is slightly stronger than the effect of production and ejection of secondary vorticity into the flow. A further interesting point from the flow visualizations and kinematic data in figure 3 is that the sphere reaches a point where it stops and reverses, implying that the fluid impulse has been recovered and is increasing. This can be reconciled with the observation that the diameter of the primary vortex core has increased during the interaction and appears to maintain its diameter once it has passed the sphere. It appears from the flow visualizations that significant secondary vorticity does not continue to be produced once the vortex ring has passed around the sphere. However care must be taken with this interpretation as no quantitative information is available for the vorticity moment during this period. The large displacement of the sphere

away from its starting position introduces the possibility of the line tension force contributing to the sphere dynamics.

5. Conclusions

This experimental study has been successful in relating, for the first time, the behaviour of the moment of vorticity to the kinematic behaviour of an object in fluid that is free to move and responds only to the forcing applied by the fluid. This has been achieved via a comparision of the experimental data with a control volume analysis to the problem of a vortex ring interacting with a sphere that is free to respond to the vortex impulse. The results for the velocity and acceleration of the sphere are in good agreement with the experimental results for the behaviour of the vorticity moment. The prediction of sphere acceleration from the rate of change of the vorticity moment are somewhat noisy, indicating the degree of precision that will be required to use this non-invasive technique to measure fluid loadings on untethered bodies in the future.

REFERENCES

ALLEN, J. J. & CHONG, M. S. 2000 Vortex formation in front of a piston moving through a cylinder. *J. Fluid Mech.* **416**, 1.

ALLEN, J. J. & AUVITY, B. 2002 Interaction of a vortex ring with a piston vortex. *J. Fluid Mech.* **465**, 453.

ALLEN, J. J. & NAITOH, T. 2005 Experimental study of the production of vortex rings using a variable diameter orifice. *Phys. Fluids* **17**, 061701.

ALLEN, J. J. & SMITS, A. J. 2001 Energy harvesting eel. *J. Fluids Struct.* **15**, 629.

GOVARDHAN, R. & WILLIAMSON, C. H. K. 2000 Modes of vortex formation and frequency response of a freely vibrating cylinder. *J. Fluid Mech.* **420**, 85.

LEONARD, A. & ROSHKO, A. 2001 Aspects of flow-induced vibration. *J. Fluids Struct.* **15**, 415.

LIGHTHILL, M. J. 1986 Fundamentals concerning wave loading on offshore structures. *J. Fluid Mech.* **173**, 667.

KELVIN, LORD 1868 On vortex motion. *Trans. R. Soc Edinb.* **25**, 217

NOCA, F., SHIELS, D. & JEON, D. 1999 A comparison of methods for evaluating time-dependent fluid dynamic forces on bodies, using only velocity fields and their derivatives. *J. Fluids Struct.* **13**, 551.

NORBURY, J. 1973 A family of steady vortex rings. *J. Fluid Mech.* **57**, 417.

ORLANDI, P. & VERZICCO, R. 1993 Vortex rings impinging on walls: axisymmetric and three-dimensional simulations. *J. Fluid Mech.* **256**, 615.

PEACE, A. J. & RILEY, N. 1983 A viscous vortex pair in ground effect. *J. Fluid Mech.* **129**, 409.

SAFFMAN, P. G. 1992 *Vortex Dynamics.* Cambridge University Press.

SHASHIKANTH, B. N. 2006 Symmetric pairs of point vortices interacting with a neutrally buoyant 2D circular cylinder. *Phys. Fluids* **18**, 127103.

SHASHIKANTH, B. N., MARSDEN J. E., BURDICK, J. W. & KELLY, S. D. 2002 The Hamiltonian structure of a 2D rigid circular cylinder interacting dynamically with N point vortices. *Phys. Fluids* **14**, 1214.

SPEDDING, G. & RIGNOT, E. 1993 Performance, analysis and application of grid interpolation techniques for fluid flows. *Exps. Fluids* **15**, 417.

TRUESDELL, C. 1954 *The Kinematics of Vorticity.* Indiana University Press.

WALKER, J. D., SMITH, C. R., CERRA, A. W. & DOGILASKI, T. L. 1987 The impact of a vortex ring on a wall. *J. Fluid Mech.* **181**, 99.